ZKG INTERNATIONAL

ISSN: 2366-1313

Mathematical Investigation of chemically reacting 3-D MHD Maxwell-Nanofluid flow across a stretching sheet in presence of Radiation effects and Multiple Slips

K. G. R. Deepthi*, S. Kavitha[1] and V. Vasudeva Murthy[2]

** Department of Mathematics, Vishnu Institute of Technology, Bhimavaram, West Godavari, 534302,Andhra Pradesh, India.*

[1] Department of Mathematics, Annamalai University, Annamalai Nagar, 608002, Tamilnadu State, India.

[2]Department of Mathematics, S. R. K. R. Engineering College, Bhimavaram, West Godavari, 534201,Andhra Pradesh, India.

**Corresponding author Email address: deepthi.k@vishnu.edu.in*

Abstract: The primary emphasis of this inquiry is a numerical evaluation of a tri-dimensional steady-state flow of viscous radiating incompressible Maxwell fluid interacting chemically approaching a stretching sheet. The investigation takes into consideration a wide range of slip effects, including those pertaining to velocity, temperature, and concentration. In this study, Using three-dimensional non-linear type similarity transformations, the controlling boundary layer equations are converted into a set of similarity equations. This was done so that the results of the investigation could be analyzed. A computer solution to the resulting equations is found by using the finite element technique. In addition, the collected data are put through a comparison analysis with findings that were previously published in particular circumstances, which reveals a high level of agreement between the two sets of data. Thirteen physical parameters, such as the parameter of the problem, Magnetic field (M), parameter of Permeability (K), Maxwell fluid component (β), parameter of Velocity slip (λ), Velocity ratio parameter (S), Prandtl number (Pr), Thermal radiation parameter (R), Thermophoresis parameter (Nt), Parameter of Brownian motion (Nb), Thermal slip parameter (δ), Schmidt number (Sc), Parameter Chemical reaction (γ), and Concentration slip parameter (ζ). As a means of providing a visual representation of the influence that a number of factors have on a variety of flow distributions, such as temperature, velocity, and concentration profiles, graphs and tables are used.

Keywords: Chemical reaction; Maxwell fluid; Magnetic field; Nanofluid; Thermal radiation; Multiple slips; Method of finite element;

Nomenclature:

Symbols List:

u, v, w **:** In the x, y and z axes,components of velocity respectively (m/s)

x, y, z **:** Measured along the stretching sheet in Cartesian coordinates (m)

f **:** stream function dimensionless along x -direction (kg / $m.\ s$)

f' **:** Through x -direction velocity of fluid's m/s)

ISSN: 2366-1313

g : Dimensionless stream function along y - direction ($kg / m.\ s$)

g' : Fluid velocity through y - direction (m/s)

Pr: Prandtl number

T: Fluid temperature (K)

V_o : Constant velocity

T_w : Temperature of the fluid (K)

T_∞ : The fluid's temperature distant from the stretched sheet (K)

Cf_x : Skin-friction coefficient along x - direction (s^{-1})

M : Magnetic field parameter

B_o : Uniform magnetic field ($Tesla$)

Cf_y : Skin-friction coefficient along y (s^{-1})

$u_w(x)$: Velocity of the fluid stretching in the x- direction (m/s)

$v_w(y)$: Fluid Velocity stretching in the y-direction (m/s)

q_w : Heat flux coefficient

q_m : Mass flux coefficient

Nt : Thermophoresis parameter

Nb : Brownian motion parameter

k^* : Permeability of porous medium

Nu_x : Heat transfer coefficient rate (or) Nusselt number

Sh_x : Mass transfer coefficient rate (or) Sherwood number

$(C_p)_{nf}$: Specific heat capacity of nano particles ($J / kg / K$)

S : Velocity ratio parameter

Re_x : Reynolds number along x - direction

Re_y : Reynolds number along y - direction

D_B : Brownian diffusion coefficient (m^2 / s)

K: Permeability component (m^{-1})

D_T : Thermophoresis diffusion coefficient

C : Fluid nanoparticle volume concentration (mol / m^3)

C_∞ : Dimensional ambient volume fraction (mol / m^3)

U_o : velocity component

L_1 : Velocity slip length

L_2 : Thermal slip length

L_3 : concentration slip length

q_r : Radiative heat flux

Kr : Non-dimensional Chemical reaction parameter

R : Parameter of Thermal radiation parameter

Sc : Schmidt number

C_w : Fluid's Dimensional concentration (mol / m^3)

K^* : Mean absorption coefficient

Greek symbols:

η : Dimensionless similarity variable (m)

θ : Dimensionless temperature (K)

ν_{nf} : Kinematic viscosity (m^2 / s)

σ_{nf} : Electrical Conductivity

ISSN: 2366-1313

ρ_{nf} : Fluid density (kg/m^3)

κ : Thermal conductivity of the fluid

τ_{wx} : shear stress on the wall along the x- axis

τ_{wy} : shear stress on the wall along the y- axis

ϕ : Dimensionless nano-fluid concentration (mol/m^3)

λ : Velocity slip parameter

δ : Thermal slip parameter

ζ : Concentration slip parameter

β_1 : Non-uniform heat transfer coefficient

β : Maxwell fluid parameter

α_m : Thermal diffusivity, (m^2/s)

τ_{wx} : Shear force acting in the x direction on the wall

τ_{wy} : Shear force acting in the y direction on the wall

σ^* : Stefan-Boltzmann constant

τ_B : Shear stress

γ : Chemical reaction parameter

Superscript:

$'$: Derivative w.r.t η

Subscripts:

nf : Nanofluid

f : Fluid

w : sheet Condition

∞ : Ambient Conditions

1. Introduction:

The study of the effects of different slip phenomena in nanofluids is an enthralling scientific topic that is still evolving within the domains of fluid dynamics and nanotechnology. The discussion of nanofluid behavior includes a variety of settings, such as microscale and nanoscale channels, the presence of solid surfaces, and other important situations. Nanofluids are colloidal suspensions of nanoparticles in base fluids. The term "slip effects" refers to the visible displacement that occurs at the interfaces that separate fluid and solid surfaces in the current framework. Because of their unusual thermal and rheological properties, nanofluids have piqued the curiosity of various application fields. Several possible applications for this technique include improving heat transport in micro-devices, lowering the temperature of electronic components, and designing more complex cooling systems. The flow of nanofluids through confined geometries includes several slip mechanisms, and the interaction between these processes can significantly impact the fluid's overall performance and behavior. The following list is a compendium of notable effects resulting from slip phenomena in nanofluids.

1. 1. Thermal Slip: Thermal slip is the occurrence of a difference of the temperature among the overall fluid temperature and the temperature at the interface between the fluid and a solid surface.

ISSN: 2366-1313

Nanoparticles have the ability to modify thermal boundary conditions, diverging from well-established heat transport principles. To achieve effective thermal management in nanofluid-based systems, it is vital to have a thorough understanding of and accurate control of thermal slip phenomena.

1. 2. Velocity slip: The idea of velocity slip refers to the relative motion observable between solid and fluid surfaces. The introduction of nanoparticles has the potential to change the gradient of the velocity at the boundary, resulting in shifts to the flow profile and slip velocities. The sliding effects may have a substantial impact on the movement of fluid dynamics and the spatial distribution of shear stress.

1. 3. Species Concentration slip: Nanoparticles have the ability to change the dynamics of mass transfer across fluid-solid interfaces in situations requiring species transportation, such as in micro-reactors or micro-fluidic devices. As a consequence, species mobility may be accelerated or reduced, which is significant in a variety of biological and chemical circumstances.

The study done by Aziz et al. [1] aimed to examine a nanofluid's dynamics in the presence of convection-induced heating on a stretched surface. The study undertaken by Battacharya and Layek [2] aimed to examine the characteristics of a nanofluid under the combined effects of a nonlinear stretching sheet and magnetic fields. The study conducted by Esfahani et al. [3] examined the characteristics of non-Newtonian nanofluids inside microchannels, with a particular focus on the thermal slip phenomenon. It has been observed that the behavior of these nanofluids differs from that of Newtonian nanofluids. In their study, Etemad and Pourfayaz [4] examined a magnetic field's impact on a stretched sheet's nanofluid flow and heat transfer properties. They explored the concurrent application of a magnetic field with several slip mechanisms, including thermal and velocity slip. The researchers exhibited a particular interest in investigating on the phenomenon of thermal slide the influence of the magnetic field. The fundamental objective of the study done by Farooq et al. [5] was around investigating the magnetohydrodynamic (MHD) movement of nanofluids in the context the production and absorption of heat processes in the surrounding environment and nonlinear thermal radiation on their publication, Ghadiri et al. [6] reported the successful development of an analytical solution that incorporates The influence of thermal slip on nanofluid flow. The Method of Adomian Decomposition (ADM) is used by researchers to facilitate the development of direct solutions for complicated issues related to fluid dynamics, which are well recognized for their inherent difficulty in obtaining such answers. In their study, Gireesha and Gorla [7] examined the phenomena of double-diffusive natural convection. This particular kind of natural convection takes place in a cavity that contains nanofluids. where fluid flow is caused by gradients in concentration and temperature working together. The fundamental objective of the study

ISSN: 2366-1313

conducted by Goodarzi et al. [8] was on investigating the transportation characteristics of Casson nanofluids through a nonlinear stretching sheet. The present study investigates the way that slip effects affect the characteristics of heat transfer and flow in Casson fluids, which are known to display non-Newtonian behavior. This measure was deemed essential due to the inherent characteristics of Casson fluids. Gupta and Gupta [9] did a research study on the impact of heat radiation on the magnetohydrodynamic (MHD) behavior of nanofluids. The study undertaken by Gupta et al. [10] centered on investigating the dynamics of unsteady magnetohydrodynamic (MHD) nanofluids flow, with particular emphasis on the influence of boundary slip conditions. The verification conducted by Haddad et al. [11] verified the phenomenon of enhanced rate of heat transmission in nanofluids flowing across a stretched surface. The study done by Jia et al. [12] investigated the heat transmission of Al_2O_3 characteristics / nanofluids water in microchannels. The research undertaken by Layek and Bhattacharyya [13] aimed to investigate the intricate interplay between magnetohydrodynamic (MHD) nanofluid flow and its many consequences. Mahmoudi et al. [14] done an investigation on slip properties of an alumina-water nanofluid's transfer of flow and heat inside a microtube, with the conditions in experimental including a constant heat flux. The study done by Mansour et al. [15] investigated the flow behavior of nanofluids under forced convection circumstances across a moving surface with convective boundary conditions. Moghaddami and colleagues [16] conducted a thorough examination of thermal slip models and heat transfer augmentation methodologies used in nanofluids confined inside microchannels. The study conducted by Olanrewaju and Sobamowo [17] examined the impact of copper-water nanofluids on heat transfer and slip flow. The researchers directed their attention on the examination of the nanofluids' behavior. The study conducted by Rehman and Nadeem [18] examined the behavior of a nanofluid under mixed convection conditions as it flowed across an inclined plate. The fundamental objective of the study undertaken by Rehman and Malik [19] was around investigating the nanofluid's flow properties near to the point of stagnation while traversing a stretched cylinder. The study done by Rehman et al. [20] verified the flow characteristics of a nanofluid subjected to joint convection while flowing across a vertically extended surface. Some of the research works ([21]-[29]) studied the multiple slip effects on nanofluid flow.

The multiple slip effects on tri-dimensional fluid flow of Maxwell over a stretched sheet The effects of heat radiation and chemical reactions have not been examined. In the previously cited literature. We developed a mathematical model to bridge this gap and used help of the finite element approach to the revised governing non-linear equations' solution. For a variety of relevant factors, graphs are displayed and explained. The Maxwell-Nanofluid characteristics of the relevant parameters have been quantitatively explored by the authors and are presented in tabular form.

ISSN: 2366-1313

Additionally, the Sherwood ,Nusselt numbers, and coefficient of skin friction are examined and shown in tables.

2. Flow Governing Equations:

In the current section, the mathematical equations of three-dimensional, electrically conductive, viscous, incompressible Maxwell fluid flow with many slips present, a porous material, and a field of magnetic approaching a stretched sheet Chemical reaction and heat radiation, Brownian motion, Nanofluid particles and Thermophoresis are derived. The physical fluid flow's geometry is explains in Fig. 1. The basic equations of this fluid flow are:

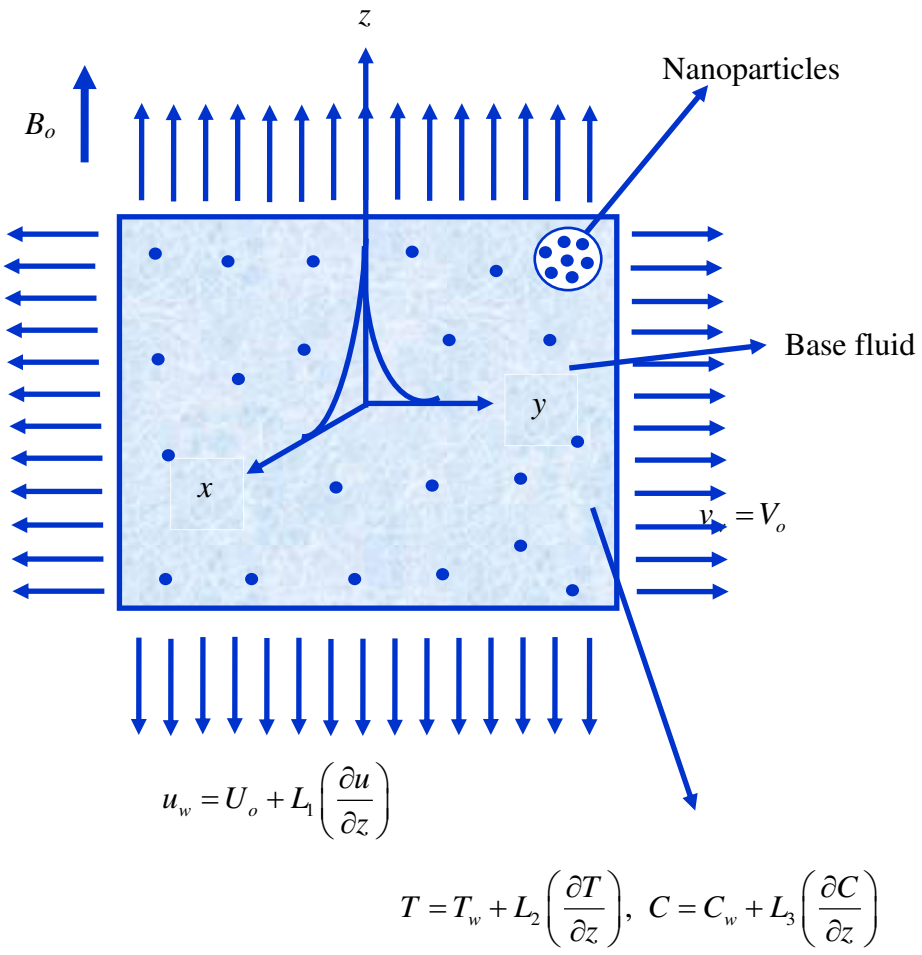

Fig. 1.: Physical representation of Maxwell-Nanofluid flow

Equation of Continuity:

$$\frac{\partial u}{\partial x}+\frac{\partial v}{\partial y}+\frac{\partial w}{\partial z}=0 \tag{1}$$

ISSN: 2366-1313

Equation of Momentum:

$$u\left(\frac{\partial u}{\partial x}\right)+v\left(\frac{\partial u}{\partial y}\right)+w\left(\frac{\partial u}{\partial z}\right)=\left(\frac{\partial^2 u}{\partial z^2}\right)-\left(\frac{\nu_{nf}}{k^*}\right)u-\left(\frac{\sigma_{nf}B_o^2}{\rho_{nf}}\right)u$$
$$-\beta_1\left\{u^2\frac{\partial^2 u}{\partial x^2}+v^2\frac{\partial^2 u}{\partial y^2}+w^2\frac{\partial^2 u}{\partial z^2}+2uv\frac{\partial^2 u}{\partial x\partial y}+2vw\frac{\partial^2 u}{\partial y\partial z}+2uw\frac{\partial^2 u}{\partial x\partial z}\right\} \quad (2)$$

$$u\left(\frac{\partial v}{\partial x}\right)+v\left(\frac{\partial v}{\partial y}\right)+w\left(\frac{\partial v}{\partial z}\right)=\left(\frac{\partial^2 v}{\partial z^2}\right)-\left(\frac{\nu_{nf}}{k^*}\right)v-\left(\frac{\sigma_{nf}B_o^2}{\rho_{nf}}\right)v$$
$$-\beta_1\left\{u^2\frac{\partial^2 v}{\partial x^2}+v^2\frac{\partial^2 v}{\partial y^2}+w^2\frac{\partial^2 v}{\partial z^2}+2uv\frac{\partial^2 v}{\partial x\partial y}+2vw\frac{\partial^2 v}{\partial y\partial z}+2uw\frac{\partial^2 v}{\partial x\partial z}\right\} \quad (3)$$

thermal energy equation :

$$u\left(\frac{\partial T}{\partial x}\right)+v\left(\frac{\partial T}{\partial y}\right)+w\left(\frac{\partial T}{\partial z}\right)=\alpha_m\left(\frac{\partial^2 T}{\partial z^2}\right)+\tau_B\left\{D_B\left(\frac{\partial T}{\partial z}\right)\left(\frac{\partial C}{\partial z}\right)+\frac{D_T}{T_\infty}\left(\frac{\partial T}{\partial z}\right)^2\right\}-\frac{1}{\left(\rho C_p\right)_{nf}}\left(\frac{\partial q_r}{\partial z}\right) \quad (4)$$

Equation of species concentration:

$$u\left(\frac{\partial C}{\partial x}\right)+v\left(\frac{\partial C}{\partial y}\right)+w\left(\frac{\partial C}{\partial z}\right)=D_B\left(\frac{\partial^2 C}{\partial z^2}\right)+\frac{D_T}{T_\infty}\left(\frac{\partial T}{\partial z}\right)^2-Kr\left(C-C_\infty\right) \quad (5)$$

The boundary conditions flows are

$$\left.\begin{aligned}&u=u_w=U_o+L_1\left(\frac{\partial u}{\partial z}\right),\ \ v=V_o,\ \ T=T_w+L_2\left(\frac{\partial T}{\partial z}\right),\ \ C=C_w+L_3\left(\frac{\partial C}{\partial z}\right)\ at\ \ z=0\\&u\to 0,\ \ T\to T_\infty,\ \ C\to C_\infty\ \ as\ \ z\to\infty\end{aligned}\right\} \quad (6)$$

flow of heat radiation q_r (using Roseland approximation) is described as

$$q_r=-\frac{4\sigma^*}{3K^*}\left(\frac{\partial T^4}{\partial z}\right) \quad (7)$$

We presume that a linear function of temperature T^4 may be used to express the expression because of the variations of temperature inside the flow. Expanding T^4 is how this is done about a free stream temperature T_∞ in a Taylor series as follows:

$$T^4=T_\infty^4+4T_\infty^3\left(T-T_\infty\right)+6T_\infty^2\left(T-T_\infty\right)^2+..... \quad (8)$$

In the above equation following the first degree term, higher-order terms in $\left(T-T_\infty\right)$, we get

$$T^4\cong 4T_\infty^3T-3T_\infty^4 \quad (9)$$

Thus substituting Eq. (9) in Eq. (7), we get

ISSN: 2366-1313

$$q_r = -\frac{16T_\infty^3\sigma^*}{3K^*}\left(\frac{\partial T}{\partial z}\right) \tag{10}$$

Using (8), Eq. (3) can be written as

$$u\left(\frac{\partial T}{\partial x}\right)+v\left(\frac{\partial T}{\partial y}\right)+w\left(\frac{\partial T}{\partial z}\right)=\alpha_m\left(\frac{\partial^2 T}{\partial z^2}\right)+\tau_B\left\{D_B\left(\frac{\partial T}{\partial z}\right)\left(\frac{\partial C}{\partial z}\right)+\frac{D_T}{T_\infty}\left(\frac{\partial T}{\partial z}\right)^2\right\}$$
$$+\frac{1}{(\rho C_p)_{nf}}\left(\frac{16T_\infty^3\sigma^*}{3K^*}\right)\left(\frac{\partial^2 T}{\partial z^2}\right) \tag{11}$$

Introducing the ensuing changes in similarity

$$\left.\begin{aligned} &u=U_o f'(\eta),\ v=V_o g'(\eta),\ \theta=\frac{T-T_\infty}{T_w-T_\infty},\ \phi=\frac{C-C_\infty}{C_w-C_\infty},\\ &w=-\sqrt{\frac{\nu_{nf}U_o}{2}}\left\{f(\eta)+\eta f'(\eta)+g(\eta)+\eta g'(\eta)\right\},\ \eta=\left(\sqrt{\frac{U_o}{2\nu_{nf}}}\right)z, \end{aligned}\right\} \tag{12}$$

Making use of Eq. (12), continuity equation (1) is uniquely satisfied and Eqs. (2), (3), (5) and (11) take the following form 8247230133

$$f'''-f'^2+ff''+gf''-Mf'-Kf'+\beta\left\{2ff'f''+2gf'f''-(f+g)^2 f'''\right\}=0 \tag{13}$$

$$g'''-g'^2+fg''+gg''-Mg'-Kg'+\beta\left\{2fg'g''+2gg'g''-(f+g)^2 g'''\right\}=0 \tag{14}$$

$$\left(1+\frac{4R}{3}\right)\theta''+\Pr f\theta'+\Pr g\theta'+\Pr Nb\theta'\phi'+\Pr Nt\theta'^2=0 \tag{15}$$

$$Nb\phi''+NbScf\phi'+NbScg\phi'+Nt\theta''-\gamma NbSc\phi=0 \tag{16}$$

the related border conditions(6) becomes

$$\left.\begin{aligned} &f(0)=0,\ g(0)=0,\ f'(0)=1+\lambda f''(0),\ g'(0)=S,\ \theta(0)=1+\delta\theta'(0),\ \phi(0)=1+\zeta\phi'(0),\\ &f'(\infty)\to 0,\ g'(\infty)\to 0,\ \theta(\infty)\to 0,\ \phi(\infty)\to 0 \end{aligned}\right\} \tag{17}$$

where the involved physical parameters are defined as

$$\left.\begin{aligned} &\beta=\beta_1 a,\ M=\frac{2\sigma_{nf}B_o^2}{\rho_{nf}U_o},\ K=\frac{2\nu_{nf}}{k^*U_o},\ S=\frac{V_o}{U_o},\ Nb=\frac{\tau_B D_B(C_w-C_\infty)}{\nu_{nf}},\ \Pr=\frac{\nu_{nf}}{\alpha_m},\ \gamma=\frac{Kr}{a},\\ &\lambda=L_1\sqrt{\frac{a}{\nu_{nf}}},\ \delta=L_2\sqrt{\frac{a}{\nu_{nf}}},\ \zeta=L_3\sqrt{\frac{a}{\nu_{nf}}},\ Nt=\frac{\tau_B D_T(T_w-T_\infty)}{\nu_{nf}T_\infty},\ Sc=\frac{\nu_{nf}}{D_B},\ R=\frac{4\sigma^*T_\infty^3}{\kappa K^*}, \end{aligned}\right\} \tag{18}$$

Quantities of physical interest, the physical characteristics of the skin-friction coefficient in the x- and y- directions, local Nusselt and Sherwood numbers are shown as follows:

$$Cf_x=\frac{2\tau_{wx}}{\rho_{nf}U_o^2}\Rightarrow Cf_x\left(\sqrt{\frac{\mathrm{Re}_x}{2}}\right)=f''(0) \tag{19}$$

ISSN: 2366-1313

$$Cf_y = \frac{2\tau_{wy}}{\rho_{nf} V_o^2} \Rightarrow \left(\sqrt{\frac{\mathrm{Re}_y}{2}}\right) Cf_y = g''(0) \tag{20}$$

$$Nu_x = \frac{xq_w}{\kappa\left(T_w - T_\infty\right)} = -\frac{x\left(\frac{\partial T}{\partial z} + \frac{\partial q_r}{\partial z}\right)_{z=0}}{\kappa\left(T_w - T_\infty\right)} \Rightarrow Nu_x = -\left(1 + \frac{4R}{3}\right)\left(\sqrt{\mathrm{Re}_x}\right)\theta'(0) \tag{21}$$

$$Sh_x = \frac{xq_m}{D_B\left(C_w - C_\infty\right)} = -\frac{x\left(\frac{\partial C}{\partial z}\right)_{y=0}}{D_B\left(C_w - C_\infty\right)} \Rightarrow \left(\sqrt{\frac{2}{\mathrm{Re}_x}}\right) Sh_x = -\phi'(0) \tag{22}$$

Where $\mathrm{Re}_x = \frac{U_o x}{\nu}$ is the local Reynolds number determined by the stretching velocity $u_w(x)$ and $\mathrm{Re}_y = \frac{V_o y}{\nu}$ is the local Reynolds number based on the stretching velocity $v_w(y)$.

3. Method of Solution by Method of Finite Element:

In sequence to address both partial, ordinary differential equations, the use of the finite element approach is necessary. This approach may be used to expeditiously solve differential equations. The concept described serves as the fundamental principle behind the finite element approach, which operates on the premise that a given region may be subdivided into discrete, finite-dimensional entities known as finite elements. At the time of authoring this manuscript, the approach described below represented the most versatile methodology for using numerical data in the field of engineering research. This methodology has been used to investigate a multitude of phenomena, including the transfer of thermal energy, the behavior of fluids, the mechanics of solids, the dynamics of rigid bodies, chemical reactions, electrical systems, and acoustic phenomena. Figure 2 illustrates the use of the finite element approach. Prior to commencing analysis by a finite element, it is essential to ensure that the following stages outlined below have been thoroughly executed:

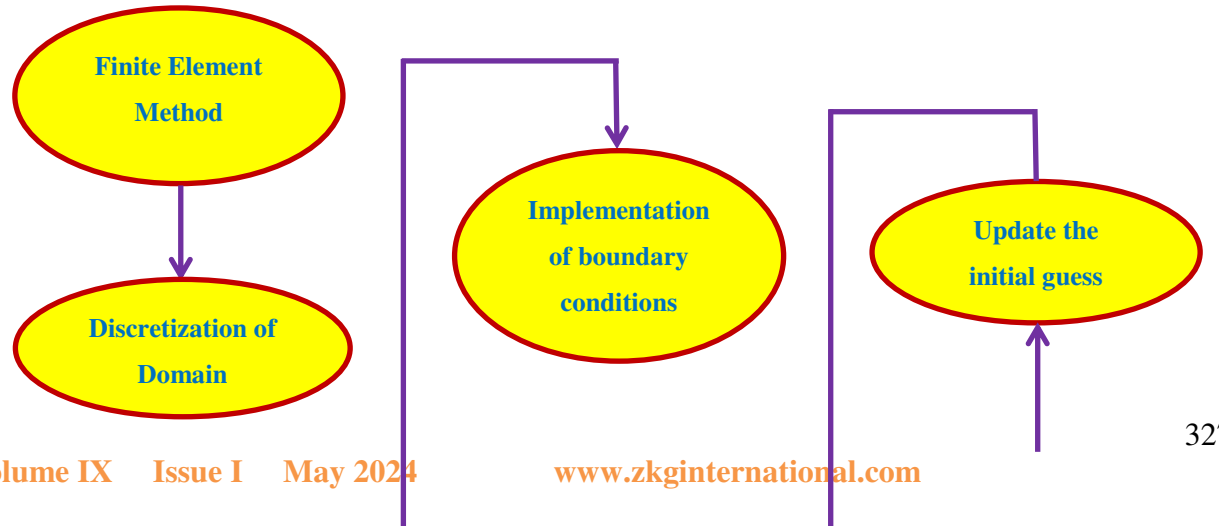

ISSN: 2366-1313

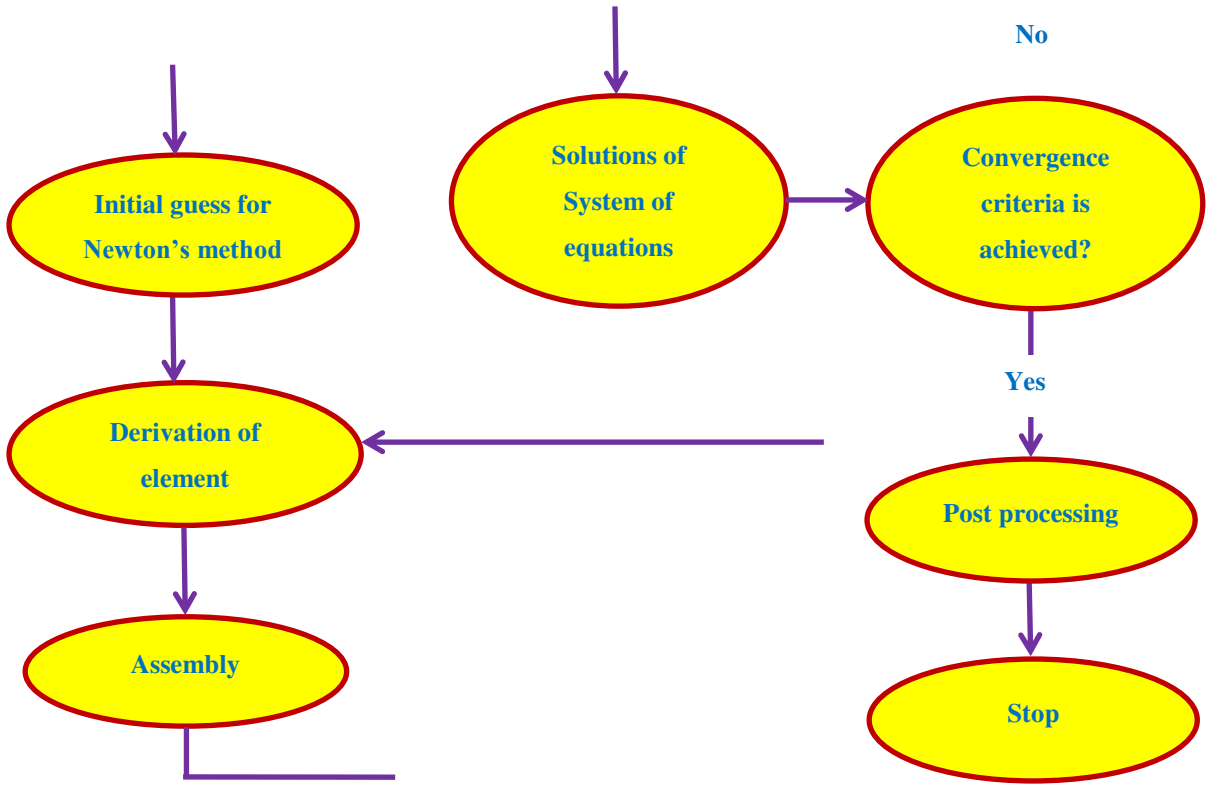

Fig. 2. Flow chart process of Finite Element

- **Domain discretization into elements:** The interval is discretized using the finite element method into a fixed number of smaller intervals, each of which is showed to as an element.
- **Domain decomposition into elements:** All of the previously listed elements make up the finite-element mesh.
- The method that follows should be used to create equations of element:

  a) Early iterations past the typical element of the mathematical model are made (one single mesh element).

  - The element equations are created by replacing the estimated solution the variational problem has an approximate solution, it is subsequently solved for the variable by integrating it into the previously constructed system.
  - Referred to as the stiffness matrix, this matrix is created by interpolating polynomials.
  - **Combining and resolving equations:** All algebraic equations must be constructed by placing restrictions on each equation's constituents regarding inter-element continuity. By tying a lot of algebraic equations together, it is feasible to create a global model of the domain using finite elements.
  - **Boundary conditions Imposition:** Applying the flow model's conditions at boundary level to the developed equations is crucial.

ISSN: 2366-1313

Various numerical methods, as the LU decomposition process and the Gauss elimination approach, may be apply to solve constructed equations. When working with real numbers, form functions are those that are used to approximate real functions. must be taken into account. The flow domain is comprised of a total of 20,001 nodes, which are further split into 10,000 quadratic components of equal dimensions. The flow domain consists of ten thousand quadratic components that are of the same size. After the element equations were created, for analysis a total of 80,004 nonlinear equations were available. The remaining system of nonlinear equations is numerically solved with an accuracy of 0.00001 using the Gauss elimination approach once the boundary conditions have been applied. The use of Gaussian quadrature facilitates the simplification of problem-solving in the context of integration. The construction of the approach's computer software was facilitated by the use of the software program MATHEMATICA, which was loaded in computer on a desktop.

4. Validation of Program Code:

Table-1.: In the x and y directions comparison of present of skin friction Coefficient results when $\beta = \lambda = M = R = \delta = \gamma = \zeta = 0$

M	Present through x-direction coefficient of Skin-friction results	Ahmad and Nazar [30] results	Present through y-direction coefficient of Skin-friction results	Ahmad and Nazar [30] results
0.0	1.0041567145699475	1.0042	0.4587879866875683	0.4653
10.0	3.3109383676783484	3.3165	1.6390871639863498	1.6459
100.0	10.048450969073164	10.0490	5.0167867437456039	5.0208

In sequence to confirm the computer code, the obtained outputs are checked and verified against the existing data in the literature, as presented by Ahmad and Nazar [30] in Table-1. This comparison and validation process serves to confirm that our numerical findings exhibit a high level of concurrence, hence showcasing the precision of our numerical results.

5. Results and Discussion:

ISSN: 2366-1313

- The changes in the parameter field of magnetic on the primary and profiles of velocity are shown in Figures 3 and 4. The Lorentz force is known resistive force that arises as the magnitude of M increases and may be considered analogous to a drag force. The Lorentz force decelerates the motion by impeding the velocity profiles.
- The impact of the Permeability coefficient for the main and secondary velocity patterns is seen in Figures 5 and 6. Depends on the numerical values, it may be inferred that is an inverse relationship among velocity profiles and the porosity parameter K, indicating a drop in velocity profiles with increasing K. This phenomenon arises when porous layer's simultaneous expansion, as K grows, the thickness of the momentum barrier layer decreases. The Maxwell fluid parameter effect (Deborah number) (K) on velocity components f' and g' are sketched in the Figures 7 and 8 respectively. The ratio of the fluid relaxation time to its characteristic time scale is known as the Deborah number. The fluid's relaxation time is the amount of time it takes to return to equilibrium after shear force is applied. It is anticipated that fluids with greater viscosities may take longer to relax. As a result, a rise in K might be interpreted as an increase in fluid viscosity, which limits fluid motion and lowers velocity. This explains why increasing K causes the hydrodynamic boundary layer to thin. It's also observed that, in contrast to two-dimensional and axi-symmetric flows, the three-dimensional flow exhibits a greater variation in the velocity fields' f' and g'.
- On display in Figure 9 is the effect that the parameter of velocity slip, denoted by λ, has on the profiles of f'. The reduction in velocity profiles is brought about by increasing the slip parameter. The inability of the nanofluid to completely acquire the stretched surface velocity during slip is the primary cause of momentum attenuation in the boundary layer, causing the velocity to drop. This is a physical phenomena known as attenuation of momentum in the boundary layer.
- Figure 10 depicts the correlation between the parameter of Velocity ratio (S) and the secondary velocity profiles. The provided figure illustrates that the secondary velocity profiles show an raising trend when the parameter of velocity ratio is increased.
- The temperature by the influence of the Prandtl number on field is seen in Figure 11. It has been observed that the Prandtl number increases (Pr) causes the thickness of the thermal layer and the temperature field to drop. Thermal diffusivity, which regulates the rate at which temperature changes, is connected to the physical quantity known as the Prandtl number (Pr). A thinner thermal layer and a decrease in the temperature field are the results of reduced thermal diffusivity with higher Prandtl numbers (Pr).

ISSN: 2366-1313

- As can be observed in Figure 12, the temperature profiles reveal oscillations that are caused by an increase in the parameter values (*R*). It is possible that the improved conduction impact of the nanofluid is to blame for the observed occurrence of a rise in fluid temperature in reaction to a rise in R. As a direct consequence of this, higher values of R are linked to greater surface heat fluxes, which ultimately outputs in higher temperatures inside the area of the boundary layer.
- Figures 13 and 14, respectively, explains the influence that the parameter of Brownian motion, *Nb*, has on the concentration and temperature curves. The temperature profiles in Figure 13 may be made to look better by the Brownian motion parameter *Nb values* increasing. These three processes are seen in Figure 13, and they cause an increase in the thermal boundary layer's thickness and temperature. A bigger parameter of Brownian motion, a lower viscous force, and a stronger Brownian diffusion coefficient all contribute to this increase. Figure 14 demonstrates that when *Nb* rises, there is a corresponding decrease in concentration.
- Figures 15 and 16 illustrate, respectively, the effect of the parameter of thermophoresis (*Nt*) on the profiles of temperature and concentration. Both of these profiles may be viewed below. The thermophoresis parameter relies on both the heat diffusion coefficient and the viscous force in order to be calculated accurately. Because of the inverse nature of the connection between the viscous force and the parameter of thermophoresis *Nt*, a rise in *Nt* results causes the viscous force to decrease and the heat diffusion coefficient to rise at the same time. As a direct consequence of these phenomena, an increase in the temperature level as well as an increase in the density of nanoparticles is produced.
- Figure 17 illustrates how temperature profiles are affected by the thermal slip parameter (δ). The profiles of temperature in this picture decrease as the parameter of thermal slip (δ) values increase.
- A temperature gradient makes it easier for mass to be transferred from a lower concentration of solute to a higher quantity of the solute. The the Schmidt number (*Sc*) impact has on concentration patterns is seen in Figure 18. The value of Sc represents the proportion of momentum to mass diffusivity. Through the use of diffusion inside the concentration boundary layer of species, one is able to arrive at the conclusion that the bonding value of mass transport and momentum may be measured. The fluid's mass diffusivity will decrease as a consequence of a rise in the *Sc* number, which will ultimately lead to a decrease in the degree to which the concentration profiles vary. Because of the inverse connection that exists between mass diffusivity and *Sc*, the Schmidt number (*Sc*) higher values are linked to lower concentration boundary layers. This is because of how Sc and mass diffusivity interact.

ISSN: 2366-1313

- Profiles on concentration the characteristic of Chemical reaction parameter (γ) are discussed in Fig. 19. As the parameter of chemical reaction increases, the profiles of concentration of the flow decrease, as the picture makes clear.
- Figure 20 depicts how the parameter slip concentration (ζ) impacts on the concentration profiles distributions. From this graph shows that when the concentration slip parameter (ζ) grows, the concentration profiles become decrease.
- The coefficient of the Skin-friction mathematical values through the x and y axes for several parameters, include, parameter of Magnetic field (M), parameter of Permeability (K), Maxwell fluid constant (β),Velocity slip (λ),Velocity ratio (S), Prandtl number (Pr),Thermal radiation (R), Thermophoresis (Nt), Brownian motion (Nb), Thermal slip (δ), Schmidt number (Sc), Chemical reaction (γ), and Concentration slip (ζ) are presented in tables- 2 and -3 respectively. From this tables, it is noticed that, the Skin-friction coefficients in the x and y directions With rising values of parameters of Velocity ratio (S), Thermal radiation (R), Thermophoresis (Nt), Brownian motion (Nb), and the reverse effect is observed in the case of parameter of Magnetic field (M), Permeability (K), Maxwell fluid (β), Velocity slip (λ), Prandtl number (Pr), Thermal slip (δ), Schmidt number (Sc), Chemical reaction (γ), and Concentration slip (ζ).
- The heat transfer coefficient rate of in terms of Nusselt number arithmetical values are displayed in Table-4 for various values of Prandtl number (Pr), parameter of Thermal radiation (R), parameter of Thermophoresis (Nt), parameter of Brownian motion (Nb), and parameter of Thermal slip (δ). The rate of heat transfer coefficient is gradually rising with increasing values of Thermal radiation parameter (R), Thermophoresis parameter (Nt), Brownian motion parameter (Nb), while the reverse impacts is verified in increasing values of Prandtl number (Pr), and Thermal slip parameter (δ).
- The rate of mass transfer coefficient numerical values in other terms of Sherwood number are displayed in Table-5 for various values of parameter of Thermophoresis (Nt), Brownian motion (Nb), Schmidt number (Sc), Chemical reaction (γ), and Concentration slip (ζ). The rate of heat transfer coefficient increases with increasing values of Thermophoresis parameter (Nt), while it decreases with increasing values of parameter of Brownian motion (Nb), Schmidt number (Sc), Chemical reaction (γ), and Concentration slip (ζ).

ISSN: 2366-1313

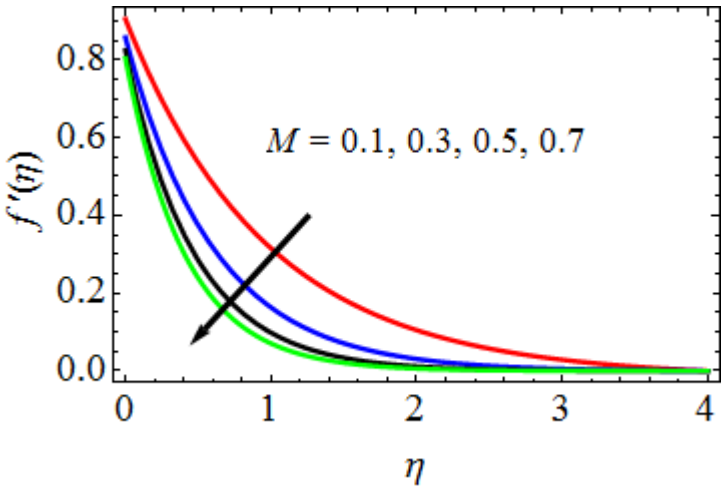

Fig. 3. *M* features on primary profiles of velocity $f'(\eta)$

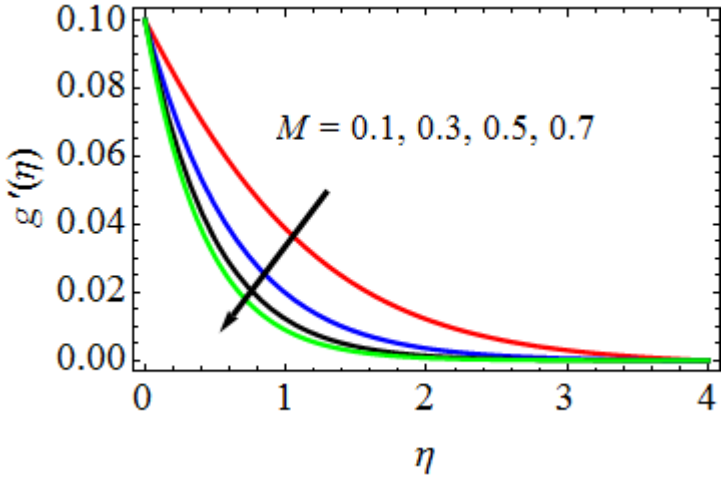

Fig. 4. *M* features on secondary profiles of velocity $g'(\eta)$

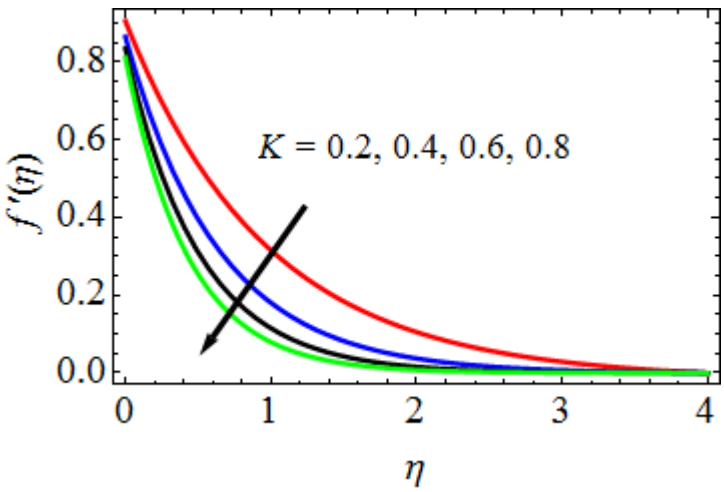

Fig. 5. *K* features on intial profiles of velocity $f'(\eta)$

ISSN: 2366-1313

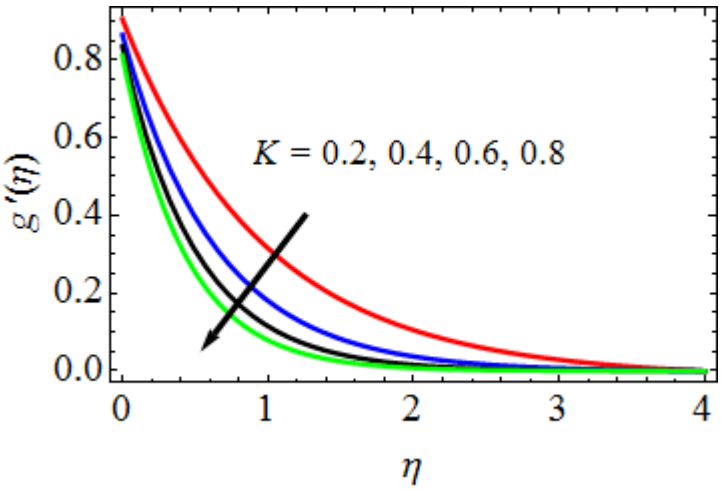

Fig. 6. K features on secondary profiles of velocity $g'(\eta)$

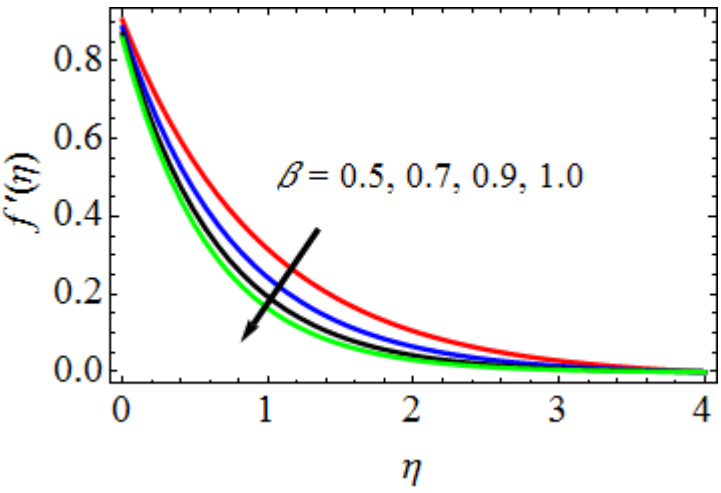

Fig. 7. β features on primary profiles of velocity $f'(\eta)$

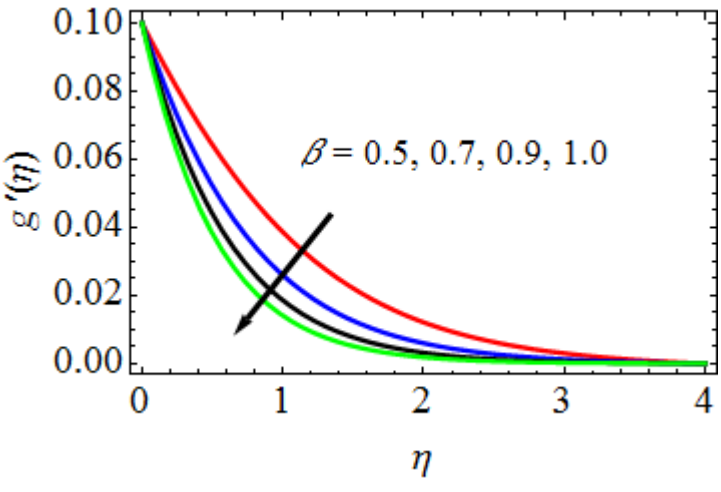

ISSN: 2366-1313

Fig. 8. β features on secondary profiles of velocity $g'(\eta)$

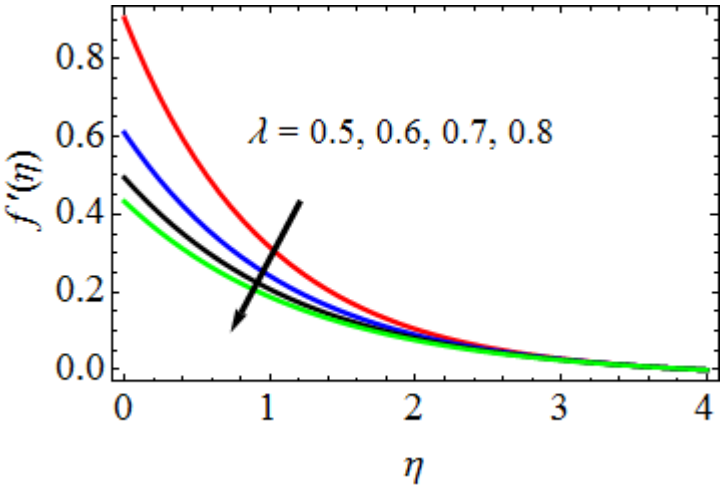

Fig. 9. λ features on primary profiles of velocity $f'(\eta)$

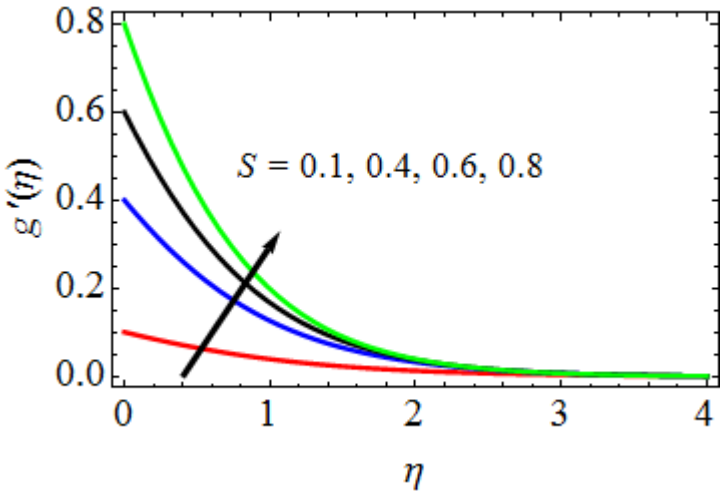

Fig. 10. S features on secondary profiles of velocity $g'(\eta)$

ISSN: 2366-1313

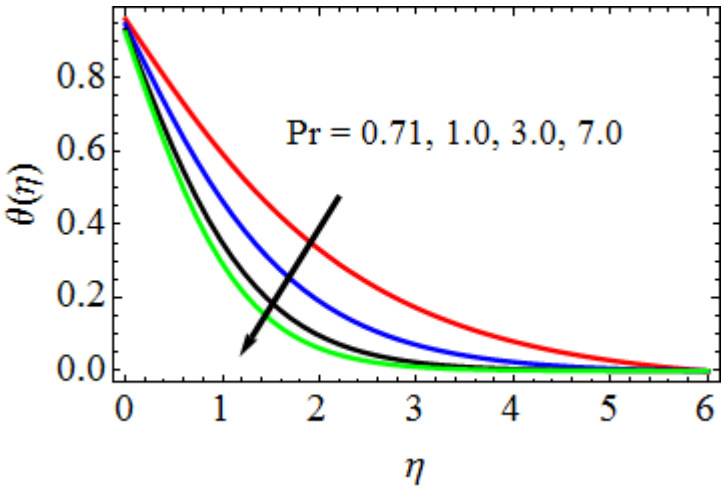

Fig. 11. Pr features on profiles of temperature $\theta(\eta)$

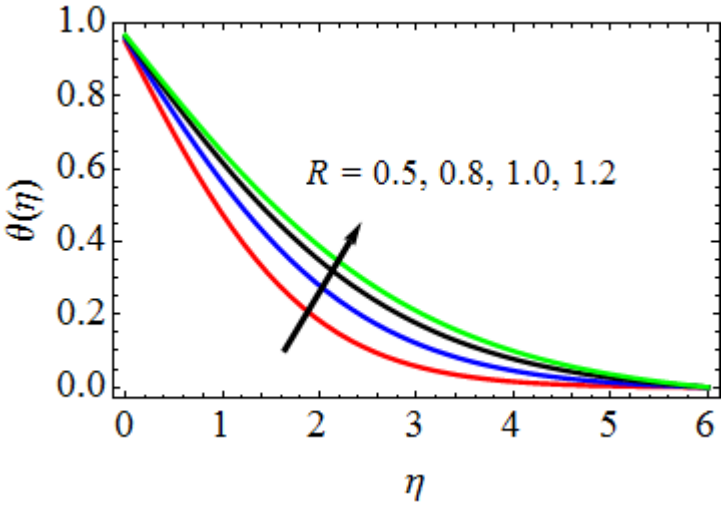

Fig. 12. *R* features on temperature profiles $\theta(\eta)$

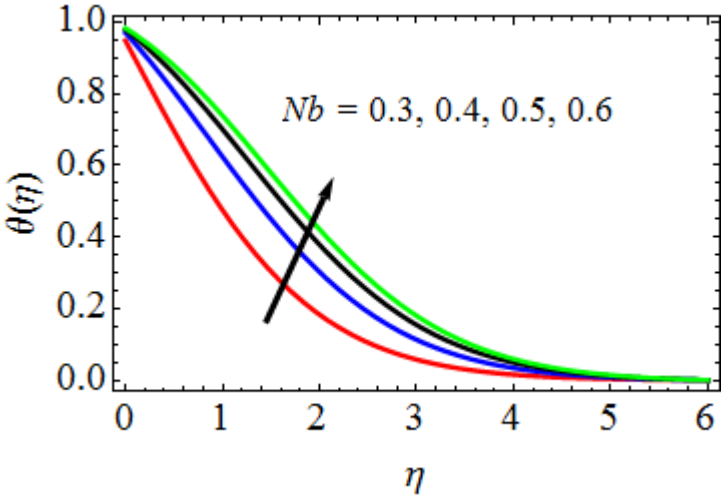

Fig. 13. *Nb* features on temperature profiles $\theta(\eta)$

ISSN: 2366-1313

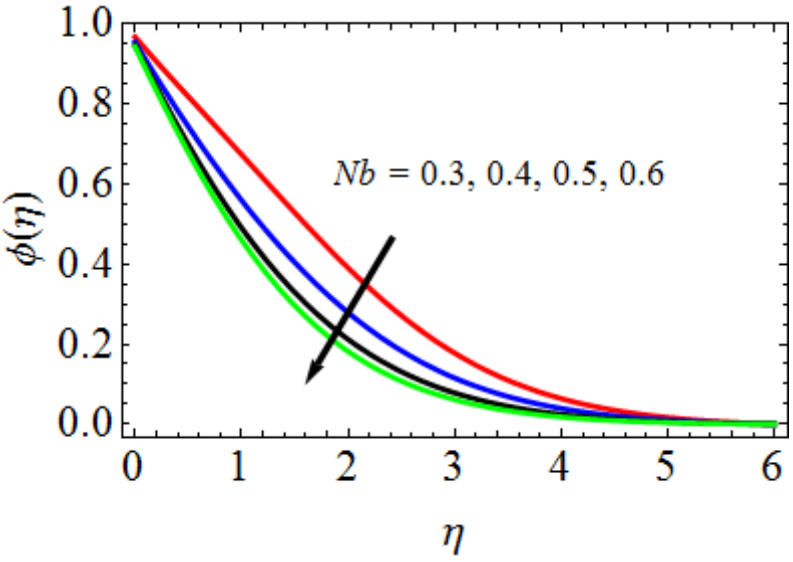

Fig. 14. *Nb* features on concentration profiles $\phi(\eta)$

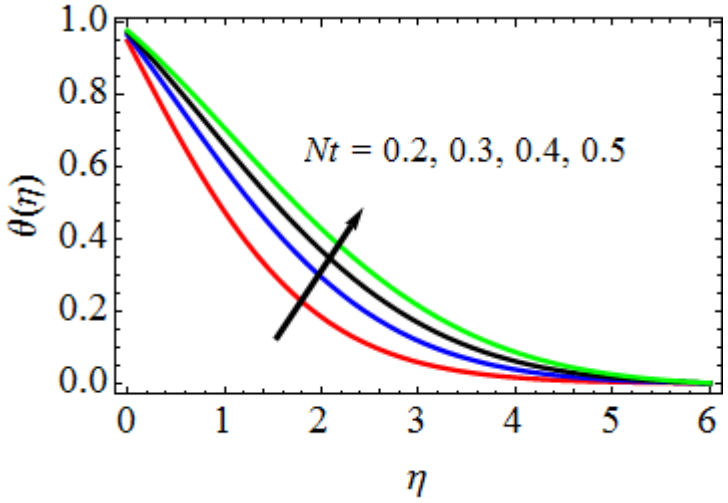

Fig. 15. *Nt* features on profiles of temperature $\theta(\eta)$

ISSN: 2366-1313

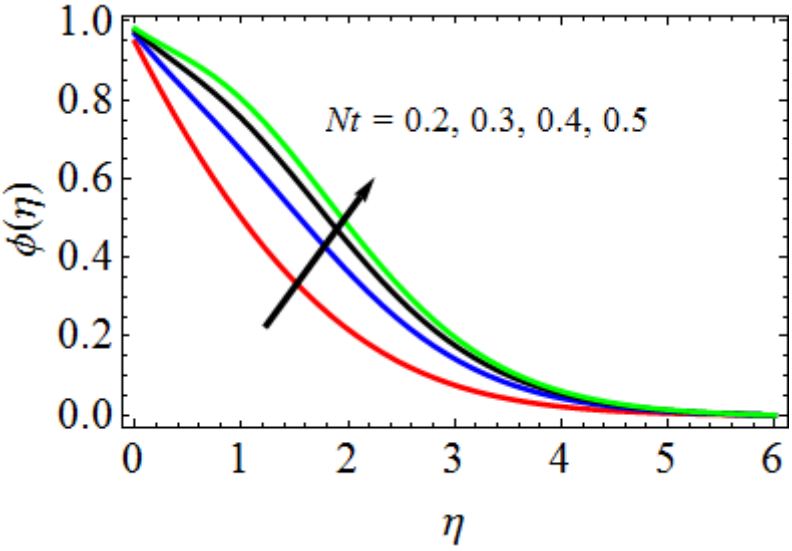

Fig. 16. *Nt* features on concentration profiles $\phi(\eta)$

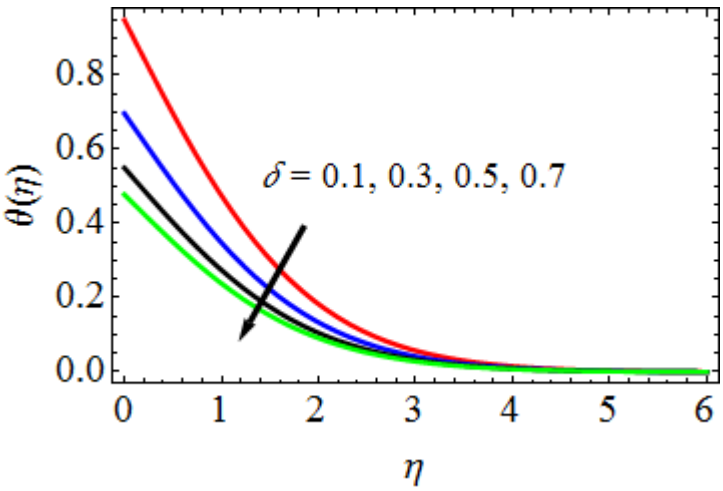

Fig. 17. δ features on temperature profiles $\theta(\eta)$

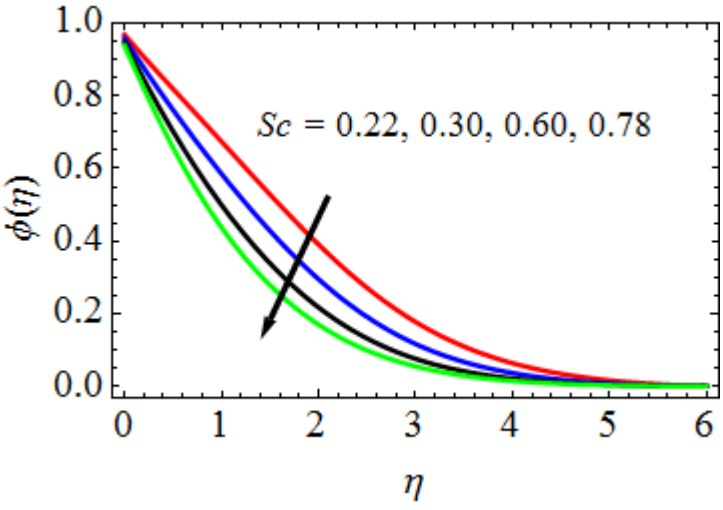

Fig. 18. *Sc* features on concentration profiles $\phi(\eta)$

ISSN: 2366-1313

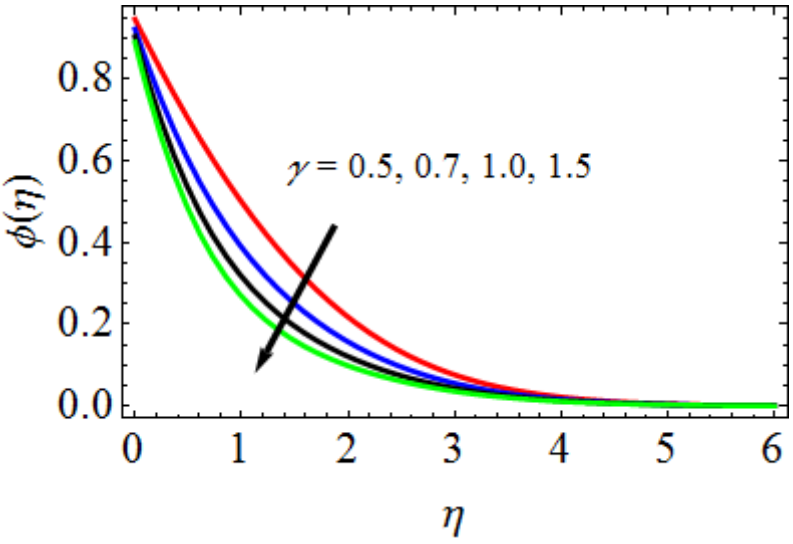

Fig. 19. γ features on temperature profiles $\theta(\eta)$

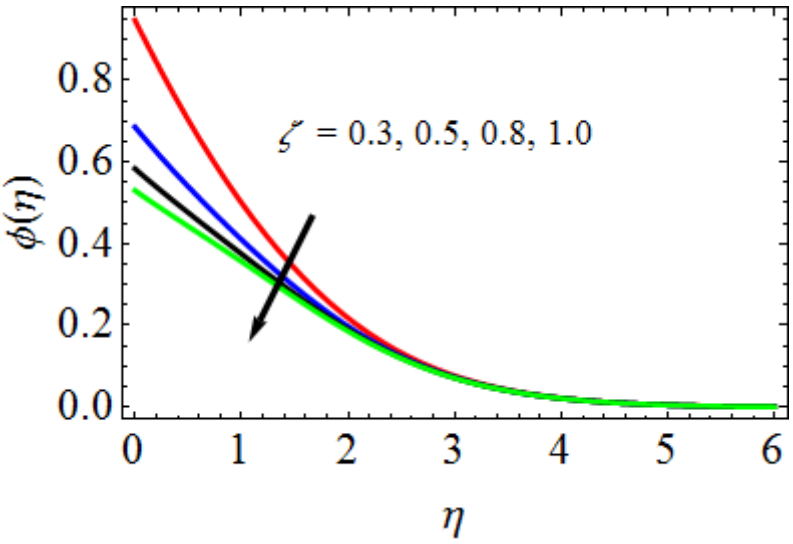

Fig. 20. ζ features on concentration profiles $\phi(\eta)$

Table-2.: Skin-friction coefficient (Cf_x) along x-direction results

M	K	β	λ	S	Pr	Nt	Nb	R	δ	Sc	γ	ζ	Cf_x
0.1	0.2	0.5	0.5	0.1	0.71	0.2	0.3	0.5	0.1	0.22	0.5	0.3	3.1565750761
0.3													3.0863760316
0.5													3.0398591378
	0.4												3.1267763811
	0.6												3.1087673787

ISSN: 2366-1313

		0.7											3.1136936343
		0.9											3.0888687093
			0.6										3.1098798583
			0.7										3.0713575494
				0.4									3.1873390939
				0.6									3.2087687369
					1.00								3.0961398675
					3.00								3.0391839837
						0.3							3.1745659830
						0.4							3.1967679396
							0.4						3.1678138967
							0.5						3.1877893093
								0.8					3.1813786302
								1.0					3.2087887985
									0.3				3.1265873013
									0.5				3.1078979837
										0.30			3.1078901684
										0.78			3.0798198695
											0.7		3.1287598131
											1.0		3.0967658706
												0.5	3.1124354874
												0.8	3.0878948945

Table-3.: Skin-friction coefficient (Cf_y) along y-direction results

M	K	β	λ	S	Pr	Nt	Nb	R	δ	Sc	γ	ζ	Cf_y
0.1	0.2	0.5	0.5	0.1	0.71	0.2	0.3	0.5	0.1	0.22	0.5	0.3	2.5166707309
0.3													2.4867869183

ISSN: 2366-1313

0.5													2.4678769359
	0.4												2.4967876987
	0.6												2.4778864569
		0.7											2.4735780180
		0.9											2.4556758936
			0.6										2.4856783719
			0.7										2.4654154433
				0.4									2.5348568413
				0.6									2.5598768019
					1.00								2.4856750364
					3.00								2.4676817509
						0.3							2.5476898735
						0.4							2.5625708730
							0.4						2.5386707304
							0.5						2.5567670691
								0.8					2.5476798457
								1.0					2.5786768736
									0.3				2.4987513703
									0.5				2.4796570848
										0.30			2.4856740309
										0.78			2.4678949878
											0.7		2.4863740334
											1.0		2.4608578679
												0.5	2.4914368763
												0.8	2.4786789137

Table-4.: Heat transfer coefficient rate of results

ISSN: 2366-1313

Pr	*Nt*	*Nb*	*R*	δ	Nu_x
0.71	0.2	0.3	0.5	0.1	0.8670987334
1.00					0.8361399345
3.00					0.8126750634
	0.3				0.8956783874
	0.4				0.9170987393
		0.4			0.8825462088
		0.5			0.9090879834
			0.8		0.8934760932
			1.0		0.9134983443
				0.3	0.8376889192
				0.5	0.8176845949

Table-5.: Rate of mass transfer coefficient results

Nt	*Nb*	*Sc*	γ	ζ	Sh_x
0.2	0.3	0.22	0.5	0.3	1.0867873591
0.3					1.1256782608
0.4					1.1476893813
	0.4				1.0498769871
	0.5				1.0278875876
		0.30			1.0467879026
		0.78			1.0056730430
			0.7		1.0165780367
			1.0		0.9868345901
				0.5	1.0267037039
				0.8	0.9767801393

6. Conclusions:

The primary reason why nanofluids are used as coolants in heat transfer appliances like heat exchangers, radiators, and electronic cooling processes is because of their exceptional thermal properties. In this research work, In the occurence of thermal radiation, chemical reaction, porous

ISSN: 2366-1313

media, and multiple slip effects, the resultant linear ordinary differential equations of magneto-hydro-dynamic Maxwell-Nanofluid flow towards a stretched sheet are numerically solved using the technique of finite element. Observing the impacts of dissimilar values of parameter of Magnetic field (M), Permeability (K), Maxwell fluid (β), Velocity slip (λ), Velocity ratio r (S), Prandtl number (Pr), Thermal radiation (R), Thermophoresis (Nt), Brownian motion (Nb), Thermal slip (δ), Schmidt number (Sc), parameter of Chemical reaction (γ), and Concentration slip (ζ) on velocity components temperature and concentration profiles, skin-friction coefficient, Nusselt and Sherwood values, and through the x and y axes. The mentioning are the ultimate findings drawn from this work:

- ✓ As the values of the Maxwell parameter of fluid, parameter of permeability, parameter of velocity slip, and parameter of magnetic field increase, the velocity profiles through the x- and y-axes decrease.
- ✓ As the velocity ratio parameter values increase, the velocity profiles thouugh the y-direction rise.
- ✓ The profiles of the temperature increase as the values of the Brownian motion, thermal radiation, and thermophoresis parameters rise, whereas the profiles of temperature decrease as the Prandtl number rises.
- ✓ With increasing values of the Schmidt number, Brownian motion parameter, chemical reaction parameter, and concentration slip parameter, the concentration profiles decrease, but when the parameter of thermophoresis is increased, the opposite trend is seen.
- ✓ In conclusion, the outcomes of the present finite element approach are excellent and, in some rare circumstances, they coincide with the results of Ahmad and Nazar [30].

References:

1. Aziz, A., Shehzad, S. A., & Abbasbandy, S. (2015). Slip effects on boundary layer flow of a nanofluid past a convectively heated stretching surface. International Journal of Heat and Mass Transfer, 85, 678-684.
2. Bhattacharyya, S., & Layek, G. C. (2015). Thermal slip effect on MHD flow and heat transfer of a nanofluid over a nonlinear stretching sheet. Journal of Molecular Liquids, 208, 290-297.
3. Esfahani, J. A., Doosthoseini, A., Ahmadi, G., & Tseng, Y. T. (2017). Thermal slip and convective heat transfer of non-Newtonian nanofluids in microchannels. Journal of Heat Transfer, 139(5), 052401.

ISSN: 2366-1313

4. Etemad, S. G., & Pourfayaz, F. (2019). Investigation of multiple slip effects on nanofluid flow and heat transfer over a stretching sheet in the presence of an applied magnetic field. International Journal of Heat and Mass Transfer, 141, 82-91.
5. Farooq, U., Hayat, T., Alsaedi, A., & Ahmad, B. (2016). On the slipping and heat generation/absorption effects in magnetohydrodynamic three-dimensional flow of nanofluid with nonlinear thermal radiation. Journal of Molecular Liquids, 216, 583-591.
6. Ghadiri, M., Layeghi, M., & Domairry, G. (2013). Analytical solution of nanofluid flow with thermal slip effect by ADM. Journal of Molecular Liquids, 188, 63-67.
7. Gireesha, B. J., & Gorla, R. S. R. (2018). Double-diffusive natural convection in a nanofluid-filled cavity with multiple slip effects. International Journal of Mechanical Sciences, 135, 256-270.
8. Goodarzi, M., Safaei, M. R., & Dahari, M. (2014). Slip effects on Casson nanofluid flow and heat transfer over a nonlinear stretching sheet. International Journal of Heat and Mass Transfer, 73, 617-624.
9. Gupta, A., & Gupta, T. (2015). Effect of slip condition on MHD flow of nanofluid in the presence of thermal radiation. *Applied Mathematics and Mechanics,* 36(12), 1547-1561.
10. Gupta, A., Gupta, T., & Pandey, M. K. (2013). Effect of thermal radiation on unsteady MHD flow of nanofluid with slip condition. *Applied Mathematics and Mechanics,* 34(3), 293-308.
11. Haddad, Z., Haddad, O., & Al-Khalidy, R. (2014). Heat transfer enhancement by multiple slip effect of nanofluids flow over a stretching surface with thermal radiation and chemical reaction. Journal of Molecular Liquids, 192, 25-30.
12. Jia, H., Nie, X., & Zheng, L. (2017). Experimental study on slip flow heat transfer of Al2O3/water nanofluids in microchannels. International Journal of Heat and Mass Transfer, 113, 1130-1140.
13. Layek, G. C., & Bhattacharyya, S. (2018). Magnetohydrodynamic nanofluid flow and heat transfer with thermal radiation and nonlinear thermal slip effects. Journal of Molecular Liquids, 256, 243-252.
14. Mahmoudi, A. H., Mahmoudi, A. H., & Ruhani, B. (2017). Slip flow and heat transfer of alumina-water nanofluid inside a microtube with constant heat flux. *Journal of Thermal Analysis and Calorimetry,* 128(2), 973-985.
15. Mansour, M. A., Saleh, H., & Ijaz, M. F. (2016). Slip effects on forced convection flow of nanofluids over a moving surface with convective boundary conditions. International Journal of Heat and Mass Transfer, 97, 1-9.

ISSN: 2366-1313

16. Moghaddami, M., Javaherdeh, K., & Safaei, M. R. (2018). A review on thermal slip models and heat transfer augmentation methods for nanofluids in microchannels. Journal of Molecular Liquids, 253, 282-297. DOI: 10.1016/j.molliq.2017.12.100
17. Olanrewaju, T., & Sobamowo, M. G. (2016). Slip flow and heat transfer of Cu-water nanofluids with and without prescribed surface temperature. Journal of Molecular Liquids, 215, 303-314.
18. Rehman, A. A., & Nadeem, S. (2018). Mixed convection flow of a nanofluid over an inclined plate with thermal radiation, chemical reaction, and slip effects. Journal of Molecular Liquids, 253, 112-121.
19. Rehman, A., & Malik, M. Y. (2019). Multiple slip effects on the stagnation point flow of nanofluid over a stretching cylinder with heat source/sink and partial slip. Applied Mathematics and Mechanics, 40(8), 1179-1188.
20. Rehman, H. U., Nadeem, S., Akbar, N. S., & Lee, C. (2017). Effects of magnetic field and nonlinear thermal slip on mixed convection flow of a nanofluid past a vertical stretching sheet. Journal of Molecular Liquids, 237, 344-351.
21. Sakiadis, B. C., & Fang, T. (2017). Slip effects on MHD flow and heat transfer over a nonlinearly stretching sheet embedded in a porous medium filled with a nanofluid. Journal of Porous Media, 20(5), 433-446.
22. Sheremet, M. A., Pop, I., & Mahian, O. (2018). Heat transfer in a micropolar nanofluid-saturated porous channel with thermal slip boundary conditions. International Journal of Heat and Mass Transfer, 127, 1379-1388.
23. Siddiqa, S., & Ahmad, S. (2016). Slip effects on unsteady boundary layer flow of a nanofluid over a permeable stretching/shrinking sheet. Journal of Molecular Liquids, 216, 273-279.
24. Turkyilmazoglu, M. (2014). Analytical solutions of nanofluid flow with thermal slip effect. International Journal of Heat and Mass Transfer, 79, 407-415.
25. Vafaei, S., Delfani, S., & Ganji, D. D. (2011). Slip effects on steady MHD nanofluid flow and heat transfer due to stretching sheet. Journal of Molecular Liquids, 159(1), 57-62. DOI: 10.1016/j.molliq.2011.02.017
26. Vajravelu, K., & Sastri, V. M. K. (2018). Slip effects on MHD flow of a nanofluid over a nonlinear stretching sheet with convective boundary condition. Journal of Nanofluids, 7(5), 854-861.
27. Yarmand, H., & Jin, L. (2011). Slip velocity modeling of nanofluid flow in porous media. International Journal of Heat and Mass Transfer, 54(7-8), 1520-1529.

ISSN: 2366-1313

28. Zhang, X., Zheng, L., & Zheng, L. (2015). Effects of thermal radiation and slip condition on mixed convection flow of a nanofluid past a stretching sheet. International Journal of Heat and Mass Transfer, 89, 1321-1327.
29. Zhang, Y., Zheng, L., Zheng, Y., & Pop, I. (2016). MHD flow and heat transfer of a nanofluid past a stretching sheet with velocity, thermal and concentration slip conditions. International Journal of Heat and Mass Transfer, 103, 355-362.
30. K. Ahmad, R. Nazar, Magnetohydrodynamic three-dimensional flow and heat transfer over a stretching surface in a viscoelastic fluid, Journal of science and technology 3 (1), (2011).